# Histological comparison of three apatitic bone substitutes with different carbonate contents in alveolar bone defects in a beagle mandible with simultaneous implant installation

Takamitsu Mano[1], Kazuya Akita[1], Naoyuki Fukuda[1], Kumiko Kamada[1], Naito Kurio[1], Kunio Ishikawa[2], Youji Miyamoto[1]

[1] Department of Oral Surgery, Institute of Biomedical Sciences, Tokushima University Graduate School, 3-18-15 Kuramotocho, Tokushima 770-8504, Japan

[2] Department of Biomaterials, Faculty of Dental Sciences, Kyushu University, 3-1-1 Maidashi, Higashi-ku, Fukuoka 812-8582, Japan

Correspondence to: Youji Miyamoto (e-mail: miyamoto@tokushima-u.ac.jp)

Tel: +81-88-633-7354 Fax: +81-88-633-7462

**Abstract**

Since bone apatite is a carbonate apatite containing carbonate in an apatitic structure, carbonate content may be one of the factors governing the osteoconductivity of apatitic bone substitutes. The aim of this study was to evaluate the effects of carbonate content on the osteoconductivity of apatitic bone substitutes using three commercially available bone substitutes for the reconstruction of alveolar bone defects of a beagle mandible with simultaneous dental implant installation. NEOBONE®, Bio-Oss®, and Cytrans® that contain 0.1 mass%, 5.5 mass%, and 12.0 mass% of carbonate, respectively, were used in this study. The amount of newly formed bone in the upper portion of the alveolar bone defect of the beagle's mandible was 0.7%, 6.6%, and 39.4% at 4 weeks after surgery and 4.7%, 39.5% and 75.2% at 12 weeks after surgery for NEOBONE®, Bio-Oss®, and Cytrans®, respectively. The results indicate that bone-to-implant contact ratio was the largest for Cytrans®. Additionally, the continuity of the alveolar ridge was restored in the case of Cytrans®, whereas the continuity of the alveolar ridge was not sufficient when using NEOBONE® and Bio-Oss®. Both Cytrans® and Bio-Oss® that has a relatively larger carbonate content in their apatitic structure was resorbed with time. We concluded that carbonate content is one of important factors governing the osteoconductivity of apatitic bone substitutes.

**Keywords**: carbonate apatite, hydroxyapatite, osteoconductivity, bone substitute

## INTRODUCTION

Bone is a composite of the inorganic component, carbonate apatite [$CO_3Ap$; $Ca_{10-a}(PO_4)_{6-b}(CO_3)_c$] and the organic components including collagen.[1] Interestingly, up to now less attention has been paid to the effect of the carbonate content in an apatitic structure of the commercially available bone substitutes on osteoconductivity or on the replacement of new bone.

Although autografts are the gold standard for the reconstruction of bone defects due to their osteoinductive, osteoconductive, and osteogenic properties, additional surgery is required for harvesting bone, and the low availability of bone as well as the complications caused by donor-site morbidity are serious drawbacks.[2] Allografts and xenografts may be potential alternatives to autografts. Since the drawbacks of these grafts such as immunogenic rejection, and the risk of disease transmission by viruses and prions are caused by the organic components, they are removed *via* thermal treatment before their use. Even though the organic components are removed by thermal treatment, the inorganic component of bone, *i.e.*, carbonate apatite, is also partially degraded due to their limited stability. In other words, carbonate apatite begins to decompose and release $CO_2$ at temperatures as low as 400°C.[3, 4] Therefore, the carbonate content of clinically available xenografts is lower when compared to the original bone.

Other alternatives for bone reconstruction are fully synthetic bone substitutes.[5-12] Among these, sintered hydroxyapatite [HAp; $Ca_{10}(PO_4)_6(OH)_2$] developed in the 1970s, represents a typical fully synthetic bone substitute. Sintered HAp is a pure ceramic and exhibits excellent tissue response and good osteoconductivity.[13, 14] Since sintered

HAp contains no organic components, immunogenic rejection and disease transmission do not occur. If sintered HAp shows a behavior similar to that of autografts, allografts, or xenografts, it could be used exclusively for bone reconstruction surgery. However, there are clear differences between the behaviors of autografts and sintered HAp. Although sintered HAp shows osteoconductivity, the degree of osteoconductivity is limited when compared to autografts. Autografts are replaced with new bone, whereas sintered HAp is not replaced by bone.[13, 14] Aside from the organic components and the growth factors contained in the organic components, HAp does not contain carbonate in its apatitic structure even though both $CO_3$Ap and HAp are classified as apatites.

Since bone apatite is the $CO_3$Ap, synthetic $CO_3$Ap is expected to exhibit properties similar to those of autogenous bone. Doi *et al.*[15] fabricated sintered $CO_3$Ap with 5.8 mass% $CO_3$ by sintering at 750°C using $CO_3$Ap powder with high proportions of $CO_3$. Unfortunately, thermal decomposition or the loss of carbonate is unavoidable. Moreover, the mechanical strength of the sintered $CO_3$Ap is low due to the low sintering temperature.

Recently, $CO_3$Ap block was fabricated in an aqueous solution by a dissolution-precipitation reaction using precursor blocks.[16-19] The $CO_3$Ap block contained a larger amount of $CO_3$ in the apatitic structure and its crystallinity was closer to that of autogenous bone when compared to sintered $CO_3$Ap or sintered HAp. The $CO_3$Ap block fabricated in an aqueous solution upregulated osteoblastic differentiation of human bone marrow cells, and was resorbed by osteoclasts.[16, 20-22]

Fujisawa *et al.*[23] reported that the $CO_3Ap$ showed faster bone formation especially in the cortical bone portion than Bio-Oss®, a bovine-derived xenograft, at 8 weeks after implantation in the bone defect of a rabbit femur. These results clearly demonstrated the potential value of the $CO_3Ap$ block as an alternative to autografts. The $CO_3Ap$ block is now commercially available as Cytrans®.

The objective of this study was, therefore, to evaluate the osteoconductivity of three apatitic bone substitutes with different carbonate contents; a fully synthetic $CO_3Ap$ fabricated in an aqueous solution (Cytrans®), a bovine-derived xenograft (Bio-Oss®), and a fully synthetic HAp (NEOBONE®). Simultaneous installation of an implant in an alveolar bone defect of a beagle dog mandible was performed.

## MATERIALS AND METHODS

### The three apatitic bone substitute granules

NEOBONE® (Coorstec, Tokyo, Japan), Bio-Oss® (Geistlich Pharma AG, Wolhusen, Switzerland), and Cytrans® (GC Corporation, Tokyo, Japan) were used as apatitic bone substitutes.

NEOBONE® is a pure HAp porous granule fabricated by the sintering method. The NEOBONE ® granules were 500 - 1000 μm in diameter. Bio-Oss® is a widely used bovine-derived xenograft. Bovine bone is treated to eliminate the organic components. The Bio-Oss® granules were 250 - 1000 μm in diameter. Cytrans® is a pure $CO_3Ap$ dense granule fabricated in an aqueous solution through a dissolution–precipitation reaction using $Ca(OH)_2$ granules as precursors.[16-19, 24] The $CO_3Ap$

granules were 300 - 600 μm in diameter.

**Scanning electron microscopic observations**

The morphology of the bone substitutes was analyzed by a scanning electron microscope (SEM) (JCM-5700, JEOL Ltd., Tokyo, Japan) under an accelerating voltage of 15 kV after coating with gold palladium using a magnetron sputtering machine (IB-3, EIKO Corporation, Tokyo, Japan).

**Compositional analysis**

The compositions of the bone substitutes were analyzed using a powder X-ray diffractometer (XRD), Fourier Transformed Infrared (FT-IR) Spectrometer. $CO_3$ content was calculated based on a C content measured using a CHN coder. For the XRD analysis, the samples were ground to fine powders, and the XRD patterns were recorded using a diffractometer (XRD; SmartLab, Rigaku Corporation, Tokyo, Japan) using CuKα radiation generated at 40 kV and 40 mA. The samples were scanned from a 2θ of 10° to 40° (where θ is the Bragg angle) in a continuous mode. Crystallite sizes were calculated from the XRD pattern using Scherrer's equation. For the FT-IR analysis, the FT-IR spectra were measured by a KBr disc method using a spectrometer (FT/IR-6200, JASCO Corporation, Tokyo, Japan). A CHN coder (MT-6; Yanako Analytical Instruments, Kyoto, Japan) was used to analyze the carbon content. Then, the carbonate contents were calculated from the carbon content as follows.

$$\text{Carbonate content (\%)} = \text{Carbon content (\%)} \times \frac{CO_3\ (60)}{C\ (12)}$$

**Porosity measurement**

Porosity of the bone substitutes was evaluated by

$$\text{Porosity } (\%) = \frac{V_p}{V_p + V_s} \times 100$$

where $V_p$ and $V_s$ are the pore volume and the volume of the samples, respectively. The pore volume of the bone substitutes was measured by a specific surface area analyzer (BELSORP-mini II, MicrotracBEL, Osaka, Japan). The volume of the samples was measured by pycnometer method, where ethanol was used as the immersion liquid.

**Dissolution rate evaluation**

The dissolution rate of the three bone substitutes was measured according to Japanese Industrial Standards T0330-3. In brief, the three bone substitutes were immersing in 0.08 mol/L pH 5.5 acetic acid-sodium acetate solution (100 mL), and 0.05 mol/L pH 7.3 tris (hydroxymethyl) aminomethane-HCl buffer solution (100 mL) at 25 ± 3°C. Sample (100 ± 1 mg) was lifted in the solution using a thread with continuous stirring. After 30 minutes, the $Ca^{2+}$ concentration in the solution was measured using a Ca ion electrode (6583-10C, Horiba, Ltd., Kyoto, Japan) as an index of dissolution rate (n = 3).

**Animal experiments**

Six male beagle dogs (weight: 8 - 11 kg) were obtained from commercial sources (Kitayama Rabesu, Nagano, Japan) and housed in the animal unit (Hamri Co., Ltd., Ibaraki, Japan) in a controlled environment. The experimental protocol was approved by the Institutional Animal Care and Use Committee (IACUC) of Hamri Co., Ltd.; IACUC approval number-No. 15-H066. The animals housed in individual cages

were provided with water and specific pellet-type laboratory animal food.

The animals were anesthetized with ketamine (10 mg/kg) and xylazine (3 mg/kg) via intramuscular injection. After local anesthesia was induced by administering 2% lidocaine containing 1:80,000 epinephrine, all mandibular premolars (first, second, third and fourth premolars) were extracted. After eight weeks of healing, mucoperiosteal flaps were elevated and bone defects 7 mm in length, 2 mm in width and 6 mm in depth were created by a fissure bur (Morita Co., Ltd., Suita, Japan) with irrigation using normal saline solution (Fig. 1a). A titanium screw type implant that was 6 mm in length and 2.2 mm in diameter was installed into the distal end of the bone defects (Fig. 1b). Thereafter, three types of bone substitutes (NEOBONE®, Bio-Oss®, and Cytrans®) were used to fill in the residual bone defects (n=3) (Fig. 1c). The surgical wound was closed with 4-0 nylon sutures. After the operation, injection of enrofloxacin (Baytril®, Bayer Medical Co., Ltd., Leverkusen, Germany) (0.4 mL/kg/10 mg) was administered intramuscularly once a day for 3 days to prevent infections and buprenorphine (20 μg/0.1 mL/kg) (Lepetan®, Otsuka Pharmaceutical Co., Ltd., Tokushima, Japan) was administered for pain relief subcutaneously to the animals once a day for 4 days. The operative sites were disinfected with povidone-iodine (Isodine®, Meiji Seika Pharma Co., Ltd., Tokyo, Japan) once a day. The sutures were removed 2 weeks after the operation.

**Histological analysis**

After 4 and 12 weeks of implantation, the animals were sacrificed using a lethal dose of intravenous pentobarbital (over 50 mg/kg). The samples along with the

surrounding tissue were carefully harvested from the mandibular bone and fixed in 10% buffered formalin for 3 days, and then dehydrated by immersion in a 70% to 100% ethanol gradient with immersion in each grade for 3 days. Finally, the samples with the surrounding tissue were embedded in methyl methacrylate. Then, undecalcified sections were prepared for histological analysis using a modified interlocked diamond saw (Exakt, Hamburg, Germany). Subsequently, Villanueva Goldner stain was applied to all sections and observed using a light microscope (BX43, OLYMPUS, Tokyo, Japan). The newly formed area of bone in the whole defect was measured using the software Image J (US National Institutes of Health, Bethesda, MD, USA). Next, the whole defect was divided into two portions (the upper portion and the lower portion) and the newly formed bone area in each portion was measured in the same manner. Bone-to-implant contact ratio was also measured using Image J as an index of osteoconductivity. Briefly, the percentage of surface length of the implant that was in direct contact with the bone was calculated. To observe the change in granule size, the areas of Bio-Oss® and Cytrans® granules in all sections were measured using Image J, and the mean areas of the Bio-Oss® and Cytrans® granules were calculated as a measure of granule size. The granule size of NEOBONE® could not be measured, because NEOBONE® has a lot of pores that form bubble-like clusters.

**Statistical analysis**

A one-way factorial ANOVA and Fisher's least significant difference post-hoc test were performed using Kaleida Graph 4 (Synergy Software Solutons Inc., PA, USA). Values are expressed as means ± standard deviations. A $p < 0.05$ value was considered

statistically significant.

## RESULTS

### Morphologic and compositional analysis

Figure 2 shows SEM images of NEOBONE® (a, d), Bio-Oss® (b, e), and Cytrans® (c, f). As shown, the structure of these three bone substitutes was different. NEOBONE® showed a typical porous structure fabricated using a spherical porogen (Fig. 2a). Higher magnification revealed the smooth surface typical of high temperature sintered ceramics (Fig. 2d).

Bio-Oss® had pores, as claimed by the manufacturer. However, as shown in Fig. 2b, the number of pores was limited when compared to those in NEOBONE®. Higher magnification revealed interwinded bundle-like structures (Fig. 2e).

In contrast to NEOBONE® and Bio-Oss®, Cytrans® was composed of dense granules (Fig. 2c). Higher magnification revealed aggregation of small crystals (Fig. 2f). In other words, the small crystals were interlocked. This structure is typical for products made *via* a dissolution–precipitation reaction such as gypsum.

Figure 3 shows the XRD patterns of NEOBONE®, Bio-Oss®, and Cytrans®. All bone substitutes demonstrated only apatitic patterns, indicating that they did not contain any other crystalline structures. For NEOBONE®, the XRD peaks were sharp indicating high crystallinity. This is typical for ceramics sintered at high temperature. In contrast, Bio-Oss® and Cytrans® demonstrated broad peaks indicating low crystallinity.

Figure 4 shows the FT-IR spectra of NEOBONE®, Bio-Oss®, and Cytrans®. Similar to XRD analysis, the FT-IR spectra also demonstrated apatitic spectra for all bone substitutes. In the case of NEOBONE®, the peak attributed to OH was observed at 638 $cm^{-1}$ (△) and no peaks attributed to carbonate were observed, indicating that NEOBONE® is a hydroxyapatite. In contrast, no absorption peak attributed to OH was observed at 638 $cm^{-1}$ for both Bio-Oss® and Cytrans®. Instead, absorption peaks at 1474, 1418 and 875 $cm^{-1}$ (▲), indicating that both Bio-Oss® and Cytrans® are AB-type $CO_3Ap$, or $CO_3Ap$ in which both A site or OH site, and B site or $PO_4$ site are replaced with $CO_3$. The absorption peaks were larger for Cytrans® when compared with Bio-Oss®, indicating that the carbonate content in apatite is larger in Cytrans® compared to Bio-Oss®.

Table 1 summarizes the chemical and physical properties of NEOBONE®, Bio-Oss®, and Cytrans®. Carbonate content is highest for Cytrans® followed by Bio-Oss® and NEOBONE®. Crystallite size is highest for NEOBONE® followed by Cytrans® and Bio-Oss®. Porosity of Bio-Oss® is more than twice larger than that of Cytrans®.

**Dissolution rate evaluation**

Figure 5 shows the results of dissolution rate evaluation. At pH 7.3 that mimicking physiological condition, all bone substitutes show limited dissolution rate even though Bio-Oss® and Cytrans® showed larger dissolution rate than NEOBONE® (Fig 5a). At pH 5.5 that mimicking inside a Howship's lacuna condition produced by osteoclasts, dissolution rate increased significantly when compared to the results of pH

7.3 regardless of the type of bone substitute. Among the bone substitutes, both Bio-Oss® and Cytrans® showed larger dissolution rate (Fig 5b).

Figure 6 shows the results of dissolution rate standardized by specific surface area. At pH 7.3, both Bio-Oss® and Cytrans® showed limited dissolution rate. At pH 5.5, Cytrans® showed statistically significant ($p < 0.01$) larger dissolution rate than that of Bio-Oss®.

**Histological analysis**

Figure 7 shows Villanueva Goldner staining in histological images of NEOBONE® (a, d), Bio-Oss® (b, e) and Cytrans® (c, f) at 4 weeks after implantation. In the case of NEOBONE®, new bone formation was observed only in the lower portion of the bone defect (Fig. 7a). Larger amounts of new bone were observed for Bio-Oss® when compared to NEOBONE®. New bone extended from the existing bone. However, little bone was formed in the central portion (Fig. 7b). The largest amount of new bone was observed when the defect was reconstructed with Cytrans®. Additionally, new bone formation was observed even in the central and upper portions (Fig. 7c). High magnification imaging revealed that new bone was not formed around the NEOBONE® granules in the central portion, and that infiltration of some lymphocytes was observed (Fig. 7d). In contrast, new bone was observed at the periphery of some of the granules in the case of Bio-Oss® (Fig. 7e). It should be noted that most of the Cytrans® granules were covered with new bone or osteoid (red) (Fig. 7f). Infiltration of few inflammatory cells and foreign body giant cells was observed in cases of Bio-Oss® and Cytrans®.

Figure 8 shows Villanueva Goldner staining in histological images of NEOBONE® (a, d), Bio-Oss® (b, e) and Cytrans® (c, f) at 12 weeks after implantation. The amount of the new bone increased when compared to 4 weeks regardless of the type of apatitic bone substitute. In the case of NEOBONE®, trabecular bone was not observed even though pores were filled with newly formed bone in the lower portion of the bone defect (Fig. 8a). At high magnification, lymphocyte infiltration decreased when compared to 4 weeks. Small amounts of new bone were observed even in the central area of the bone defect (Fig 8d). In the case of Bio-Oss®, larger amounts of new bone were observed in the central area when compared to NEOBONE®. However, the continuity of the alveolar ridge was not restored (Fig. 8b). At high magnification, some Bio-Oss® granules covered with new bone were observed (Fig. 8e). In the case of Cytrans®, new bone was formed uniformly all over the bone defect and the continuity of the alveolar ridge was restored (Fig. 8c). The new bone was in direct contact with the granules without the presence of an intermediate layer of fibrous tissue and most of the granules were covered with new bone (Fig. 8f). The osteoid was gradually replaced with mature bone and cuboidal osteoblasts indicating activated osteoblasts, were present on the surface of the osteoid. The size of the Bio-Oss® and Cytrans® granules at 12 weeks was smaller than that at 4 weeks.

Figure 9 shows the percentage of new bone in the whole bone defect. The percentages of new bone in NEOBONE®, Bio-Oss® and Cytrans® at 4 weeks after implantation were 6.5 ± 3.3%, 17.9 ± 4.2% and 42.2 ± 19.4%, respectively. The area of new bone was significantly larger for Cytrans® and Bio-Oss® than in NEOBONE®.

The percentage of new bone in NEOBONE®, Bio-Oss® and Cytrans® at 12 weeks after implantation were 25.7 ± 6.0%, 41.5 ± 1.9% and 61.9 ± 5.3%, respectively. The area of new bone increased at 12 weeks when compared to 4 weeks regardless of the type of bone substitute. Moreover, the order of the amount of new bone was the same as that observed at 4 weeks. Significantly larger amounts of new bone were observed for Cytrans® when compared to NEOBONE® and Bio-Oss®.

Figure 10 shows the percentage of the new bone areas in the upper portion (alveolar ridge portion; 10a) and in the lower portion (bone marrow portion; 10b), at 4 and 12 weeks after implantation. The trend shown by the formation of new bone was the same as that shown in Figure 9. However, the differences in the new bone formation area based on the type of bone substitute were much more significant in the upper portion. In the upper portion, the areas of new bone formation for NEOBONE®, Bio-Oss® and Cytrans® at 4 and 12 weeks after implantation were 0.7 ± 0.3%, 6.6 ± 7.2%, 39.4 ± 15.0% and 4.7 ± 4.9%, 39.5 ± 26.9% and 75.2 ± 5.7%, respectively. In the lower portion, the areas of new bone formation for NEOBONE®, Bio-Oss®, and Cytrans® at 4 and 12 weeks after implantation were 12.0 ± 6.5%, 28.9 ± 4.9%, and 45.6 ± 26.9%, and 46.1 ± 14.2%, 45.4 ± 29.4%, and 51.5 ± 9.2%, respectively.

Figure 11 shows the histological images of the titanium implant surface when implanted adjacent to the bone defect filled with NEOBONE® (a, d), Bio-Oss® (b, e) and Cytrans® (c, f) for 4 weeks (a - c) and 12 weeks (d - f). At 4 weeks, in the case of NEOBONE®, the titanium implant was barely in contact with the new bone (Fig. 11a). In the case of Bio-Oss® (Fig. 11b) and Cytrans® (Fig. 11c), the titanium implant was in

direct contact with the new bone. At 12 weeks, the bone-to-implant contact area increased when compared to 4 weeks regardless of the type of bone substitute. In the case of NEOBONE® and Bio-Oss®, the titanium implant was in partial contact with the new bone (Fig. 11d, e). In contrast, for Cytrans®, most of the titanium implant surface was covered with the new bone (Fig. 11f).

Figure 12 shows the percentage of the bone-to-implant contact ratio. The contact ratios of NEOBONE®, Bio-Oss® and Cytrans® were 2.2 ± 2.1%, 13.4 ± 5.4%, 19.4 ± 12.4%, and 36.6 ± 6.9%, 37.2 ± 10.8%, 62.3 ± 8.0%, after 4 and 12 weeks, respectively. The bone-to-implant contact ratios increased with time regardless of the bone substitute used to fill the adjacent bone defect. Cytrans® showed a significantly higher bone-to-implant contact ratio than NEOBONE® and Bio-Oss® at 12 weeks.

Figure 13 summarizes the resorption of the Bio-Oss® and Cytrans® granules using granule area as an index. The mean area of Bio-Oss® was 0.103 ± 0.064 $mm^2$, 0.073 ± 0.072 $mm^2$ and 0.065 ± 0.076 $mm^2$ at 0, 4 and 12 weeks, respectively. In addition, the mean area of the Cytrans® granules was 0.091 ± 0.057 $mm^2$, 0.074 ± 0.058 $mm^2$, and 0.054 ± 0.040 $mm^2$ at 0, 4, and 12 weeks, respectively. Both Bio-Oss® and Cytrans® granules were gradually resorbed with time even though statistically significant differences were not recognized.

## DISCUSSION

Results obtained in this study clearly demonstrated the usefulness of $CO_3$Ap bone substitute with larger $CO_3$ content in apatitic structure. As well known, new bone is

formed from the existing bone and/or the periosteum. Osteoblasts in existing bone and/or periosteum are upregulated thus forming greater amounts of bone. In other words, Cytrans® that contains 12.0 ± 0.6 mass% $CO_3$ showed the highest rate of bone formation among the three apatitic bone substitutes. The bone formation rate followed by Bio-Oss® that contains 5.5 ± 0.2 mass% $CO_3$, and NEOBONE® that contains 0.1 ± 0.1 mass% $CO_3$. Clearest difference on the new bone formation was observed in the upper portion of the alveolar bone defect. For Cytrans®, new bone formation derived from the periosteum is observed in the upper portion of the alveolar bone defect. It should be noted that the upper portion of the alveolar bone defect is the last part derived from the existing bone.

As a results of greater amount of new bone formation, higher bone-to-implant contact ratio was observed when the adjacent bone defect was filled with Cytrans® (Figs. 11,12). The newly formed bone bonded to the titanium implant because of titanium's osteointegration ability.

These results are not only fruitful to patients but also allow great chance to understand factors to determine the osteoconductivity. Obviously, $CO_3$ content in apatitic structure and the percentage of new bone in the whole bone defect correlate well. The formers are 0.1 ± 0.1 mass%, 5.5 ± 0.2 mass%, 12.6 ± 0.6 mass%, and the latters are 6.5 ± 3.3%, 17.9 ± 4.2%, 42.2 ± 19.4% in 4 weeks and 25.7 ± 6.0%, 41.5 ± 1.9% and 61.9 ± 5.3% in 12 weeks for NEOBONE®, Bio-Oss® and Cytrans®, respectively. The results are consistent with the previous results. Germaini *et al.*[25] reported that 4.4 wt% carbonate substituted hydroxyapatite promoted a significantly

higher level of pre-osteoblast proliferation than HAp containing no $CO_3$ in apatitic structures. Nagai *et al*.[20] also reported that $CO_3$Ap upregulated the osteoblastic differentiation of cultured human bone marrow cells when compared to HAp.

One of the causes of the higher osteoconductivity for bone substitutes with larger $CO_3$ content in apatitic structure may be larger solubility at the weak acidic condition produced by osteoclasts, and resulting upregulation of osteoblasts by $Ca^{2+}$. It is well known that the solubility of apatite in weak acidic conditions increases with $CO_3$ content in apatitic structures.[26] Therefore, osteoclastic resorption increases with $CO_3$ content in apatitic structures because Howship's lacuna produced by osteoclasts represents a weak acidic environment. In fact, Spence *et al*.[21] reported that higher carbonate content led to an increased osteoclastogenesis and allowed resorption of the substitute in a dose dependent manner *in vivo*. Further, Fujisawa *et al*.[23] reported that the size of the $CO_3$Ap granules became smaller with implantation time *in vivo*. The resorption of bone or dissolution of apatite elevates $Ca^{2+}$ concentration since both bone and apatite are composed of calcium-phosphate. Lee *et al*.[27] reported that elevated extracellular $Ca^{2+}$ enhanced osteoblastic differentiation in cultured murine osteoblasts, including the expression and secretion of osteopontin and matrix mineralization. Maeno *et al*.[28] also demonstrated that a $Ca^{2+}$ concentration of about 5 mM, which is higher than the physiological concentration (2.1 - 2.5 mM in human serum), is appropriate for proliferation and differentiation of cultured mouse osteoblasts. Therefore, elevated $Ca^{2+}$ supplied by the resorption of bone or dissolution of apatite may be one of key factors for new bone formation, and $CO_3$ content in apatitic

structures may be one of keys for new bone formation.

Although histological comparison of the commercially available bone substitutes is important, there are dissimilarities other than $CO_3$ contents. Obviously, porous structure is one of the factors to determine the function of bone substitute. As shown in Fig. 2, NEOBONE® is porous whereas Cytrans® is dense. Since Cytrans® shows much higher osteoconductivity than NEOBONE®, compositional factor seems more important than porous structure. NEOBONE®, a porous HAp containing 0.1 ± 0.1 mass% $CO_3$ in its apatitic structures, showed limited dissolution rate at pH 5.5 (Fig. 5), and was not resorbed at the site of bone defect. Therefore, $Ca^{2+}$ elevation at the bone defect is limited leading the lowest osteoconductivity.

Comparison of the Cytrans® and Bio-Oss® is more complex. $CO_3$ content of Cytrans® and Bio-Oss® are 12.0 ± 0.6 mass% and 5.5 ± 0.2 mass%, respectively. When dissolution rate is standardized by specific surface area, dissolution rate of Cytrans® is larger than that of Bio-Oss® as shown in Fig. 6. However, dissolution rates at pH 5.5 solution without standardization by specific surface area are the same as shown in Fig. 5. Therefore, osteoclastic resorption may be the same and resulting $Ca^{2+}$ elevation and upregulation of osteoblasts may be the same. There are other dissimilarities including the crystallite size, surface morphology and method of fabrication. They may be factors to determine the osteoconductivity. $CO_3$ content in apatitic structure may directly influence the osteoconductivity. In fact, papers of Germaini *et al.*[25] and Nagai *et al.*[20] reported upregulation of proliferation and differentiation by $CO_3$Ap than HAp, detailed mechanism of upregulation was not

clarified. Further factor analysis on osteoconductivity is awaited based on the results obtained in this study.

## CONCLUSION

In summary, Cytrans® granules that are fabricated in an aqueous solution and have the largest $CO_3$ content exhibited the highest rate of bone formation and the highest bone-to-implant contact ratio in the alveolar bone defect of a dog mandible with simultaneous implant installation when compared to NEOBONE® and Bio-Oss®. The results obtained in this study suggest that $CO_3$ content may be one of the factors governing bone formation and resorption in bone defects.


## Acknowledgements

This research was supported by AMED under Grant Number JP18im0502004.


## Conflict of interest

This animal experiment was, in part, funded by GC Corporation (Tokyo, Japan). However, GC Corporation had no further participation in conducting of the study, and exerted no control over the interpretation, authoring, or publication of the results of this work.

## REFERENCES


1. Abou Neel EA, Aljabo A, Strange A, Ibrahim S, Coathup M, Young AM, Bozec L,

Mudera V. Demineralization-remineralization dynamics in teeth and bone. Int J Nanomedicine 2016; 11: 4743-4763.

2. Miron RJ, Zhang YF. Osteoinduction: a review of old concepts with new standards. J Dent Res 2012; 91: 736-744.
3. Rau JV, Cesaro SN, Ferro D, Barinov SM, Fadeeva IV. FTIR study of carbonate loss from carbonated apatites in the wide temperature range. J Biomed Mater Res B Appl Biomater 2004; 71: 441-447.
4. Landi E, Tampieri A, Celotti G, Vichi L, Sandri M. Influence of synthesis and sintering parameters on the characteristics of carbonate apatite. Biomaterials 2004; 25:1763-1770.
5. Daculsi G, Passuti N, Martin S, Deudon C, Legeros RZ, Raher S. Macroporous calcium phosphate ceramic for long bone surgery in humans and dogs. Clinical and histological study. J Biomed Mater Res 1990; 24: 379-396.
6. Frayssinet P, Trouillet JL, Rouquet N, Azimus E, Autefage A. Osseointegration of macroporous calcium phosphate ceramics having a different chemical composition. Biomaterials 1993; 14: 423-429.
7. de Groot K. Bioceramics consisting of calcium phosphate salts. Biomaterials 1980; 1: 47-50.
8. Miyamoto Y, Ishikawa K, Takechi M, Toh T, Yuasa T, Nagayama M, Suzuki K. Basic properties of calcium phosphate cement containing atelocollagen in its liquid or powder phases. Biomaterials 1998; 19: 707-715.
9. Yuasa T, Miyamoto Y, Ishikawa K, Takechi M, Momota Y, Tatehara S, Nagayama

M. Effects of apatite cements on proliferation and differentiation of human osteoblasts in vitro. Biomaterials 2004; 25: 1159-1166.

10. Bhatnagar RS, Qian JJ, Wedrychowska A, Sadeghi M, Wu YM, Smith N. Design of biomimetic habitats for tissue engineering with P-15, a synthetic peptide analogue of collagen. Tissue Eng 1999; 5: 53-65.
11. Yang XB, Roach HI, Clarke NM, Howdle SM, Quirk R, Shakesheff KM, Oreffo RO. Human osteoprogenitor growth and differentiation on synthetic biodegradable structures after surface modification. Bone 2001; 29: 523-531.
12. Endres M, Hutmacher DW, Salgado AJ, Kaps C, Ringe J, Reis RL, Sittinger M, Brandwood A, Schantz JT. Osteogenic induction of human bone marrow-derived mesenchymal progenitor cells in novel synthetic polymer-hydrogel matrices. Tissue Eng 2003; 9: 689-702.
13. Moore WR Graves SE, Bain GI. Synthetic bone graft substitutes. ANZ J Surg 2001; 71: 354-361.
14. Kattimani VS, Chakravarthi PS, Prasad LK. Biograft block hydroxyapatite: A ray of hope in the reconstruction of maxillofacial defects. J Craniofac Surg 2016; 27: 247-252.
15. Doi Y, Shibutani T, Moriwaki Y, Kajimoto T, Iwayama Y. Sintered carbonate apatites as bioresorbable bone substitutes. J Biomed Mater Res 1998; 39: 603-610.
16. Ishikawa K. Bone substitute fabrication based on dissolution-precipitation reactions. Materials 2010; 3: 1138–1155.
17. Lin X, Matsuya S, Udoh K, Nakagawa M, Terada Y, Ishikawa K. Fabrication of

calcium carbonate monolith by carbonation of calcium hydroxide compact, Archives Bioceram Res 2003; 3: 83-88.

18. Ishikawa. K, Matsuya S, Lin X, Lei Z, Yuasa T, Miyamoto Y. Fabrication of low crystalline B-type carbonate apatite block from low crystalline calcite block. J Ceram Soc Jpn 2010; 118: 341-344.
19. Wakae H, Takeuchi A, Udoh K, Matsuya S, Munar ML, LeGeros RZ, Nakasima, A, Ishikawa K. Fabrication of macroporous carbonate apatite foam by hydrothermal conversion of alpha-tricalcium phosphate in carbonate solutions. J Biomed Mater Res A. 2008; 87: 957-963.
20. Nagai H, Kobayashi-Fujioka M, Fujisawa K, Ohe G, Takamaru N, Hara K, Uchida D, Tamatani T, Ishikawa K, Miyamoto Y. Effects of low crystalline carbonate apatite on proliferation and osteoblastic differentiation of human bone marrow cells. J Mater Sci Mater Med 2015; 26: 99.
21. Spence G, Patel N, Brooks R, Bonfield W, Rushton N. Osteoclastogenesis on hydroxyapatite ceramics: the effect of carbonate substitution. J Biomed Mater Res A 2010; 92: 1292-1300.
22. Kanayama K, Sriarj W, Shimokawa H, Ohya K, Doi Y, Shibutani T. Osteoclast and osteoblast activities on carbonate apatite plates in cell cultures. J Biomater Appl 2011; 26: 435-449.
23. Fujisawa K, Akita K, Fukuda N, Kamada K, Kudoh T, Ohe G, Mano T, Tsuru K, Ishikawa K, Miyamoto Y. Compositional and histological comparison of carbonate apatite fabricated by dissolution-percipitation reaction and Bio-Oss®. J Mater Sci

Mater Med 2018; 29: 121.

24. Lin X, Matsuya S, Nakagawa M, Terada Y, Ishikawa K. Effect of molding pressure on fabrication of low-crystalline calcite block. J Mater Sci Mater Med 2008; 19: 479-484.

25. Germaini MM, Detsch R, Grünewald A, Magnaudeix A, Lalloue F, Boccaccini AR, Champion E. Osteoblast and osteoclast responses to A/B type carbonate-substituted hydroxyapatite ceramics for bone regeneration. Biomed Mater. 2017; 12: 035008.

26. LeGeros RZ, Tung MS. Chemical stability of carbonate- and fluoride-containing apatites. Caries Res 1983; 17: 419-429.

27. Lee MN, Hwang HS, Oh SH, Roshanzadeh A, Kim JW, Song JH, Kim ES, Koh JT. Elevated extracellular calcium ions promote proliferation and migration of mesenchymal stem cells via increasing osteopontin expression. Exp Mol Med 2018; 50: 142.

28. Maeno S, Niki Y, Matsumoto H, Morioka H, Yatabe T, Funayama A, Toyama Y, Taguchi T, Tanaka J. The effect of calcium ion concentration on osteoblast viability, proliferation and differentiation in monolayer and 3D culture. Biomaterials 2005; 26: 4847–4855.

**Figure captions**

FIGURE 1. Surgical procedures for the creation of the bone defect, installation of the implant, and filling of the bone substitutes in the alveolar bone defect.

Eight weeks after extraction of the premolars, bone defects of 7 mm in length, 2

mm in width, and 6 mm in depth were created by using a fissure bur at the premolar region (a), screw type titanium implants were installed into the distal end of each bone defect (b), each of the bone substitutes was placed in the residual bone defect (c).

FIGURE 2. Scanning electron micrograph images of NEOBONE® (a), Bio-Oss® (b) and Cytrans® (c) at low magnification, and high magnification of NEOBONE® (d), Bio-Oss® (e), and Cytrans® (f)

FIGURE 3. X-ray diffraction patterns of NEOBONE® (a), Bio-Oss® (b) and Cytrans® (c)

Black circles indicate the peaks of the HAp.

FIGURE 4. FT-IR spectrum of NEOBONE® (a), Bio-Oss® (b) and Cytrans® (c)

Black triangles (▲) indicate the peaks attributed to $CO_3$. White triangle (△) indicate the peak attributed to OH.

FIGURE 5. Dissolution rates of NEOBONE®, Bio-Oss® and Cytrans® in pH 7.3 buffer solution (a) and in pH 5.5 buffer solution (b). **$p < 0.01$

FIGURE 6. Dissolution rates of NEOBONE®, Bio-Oss® and Cytrans® standardized by specific surface area in pH 7.3 buffer solution (a) and in pH 5.5 buffer solution (b). **p < 0.01

FIGURE 7. Histological views of the graft areas of NEOBONE® (a, d), Bio-Oss® (b, e) and Cytrans® (c, f) at 4 weeks after implantation (Villanueva Goldner stain). Newly formed bone (NB) was stained green, and the osteoid was stained red. Asterisks indicate Bio-Oss® and Cytrans® granules.

FIGURE 8. Histological views of the graft areas of NEOBONE® (a, d), Bio-Oss® (b, e) and Cytrans® (c, f) at 12 weeks after implantation. Arrowheads indicate osteoblasts observed on the surface of the osteoid.

FIGURE 9. Percentage of new bone area in the whole area of the bone defect at 4 and 12 weeks after implantation. *p < 0.05, **p < 0.01

FIGURE 10. Percentage of new bone area in the upper portion (a) and lower portion (b) at 4 and 12 weeks after implantation. *p < 0.05, **p < 0.01

FIGURE 11. Histological views of the titanium implant surface adjacent to bone defect filled with NEOBONE® (a, d), Bio-Oss® (b, e) and Cytrans® (c, f) at 4, and 12 weeks after implantation.

FIGURE 12. Bone-to-implant contact ratio of titanium implant adjacent to bone defect filled with NEOBONE®, Bio-Oss® and Cytrans® at 4, and 12 weeks after implantation. **$p < 0.01$

FIGURE 13. Mean area of granules at the bone defect filled with Bio-Oss® and Cytrans® at 0, 4 and 12 weeks after implantation.


a
b
c

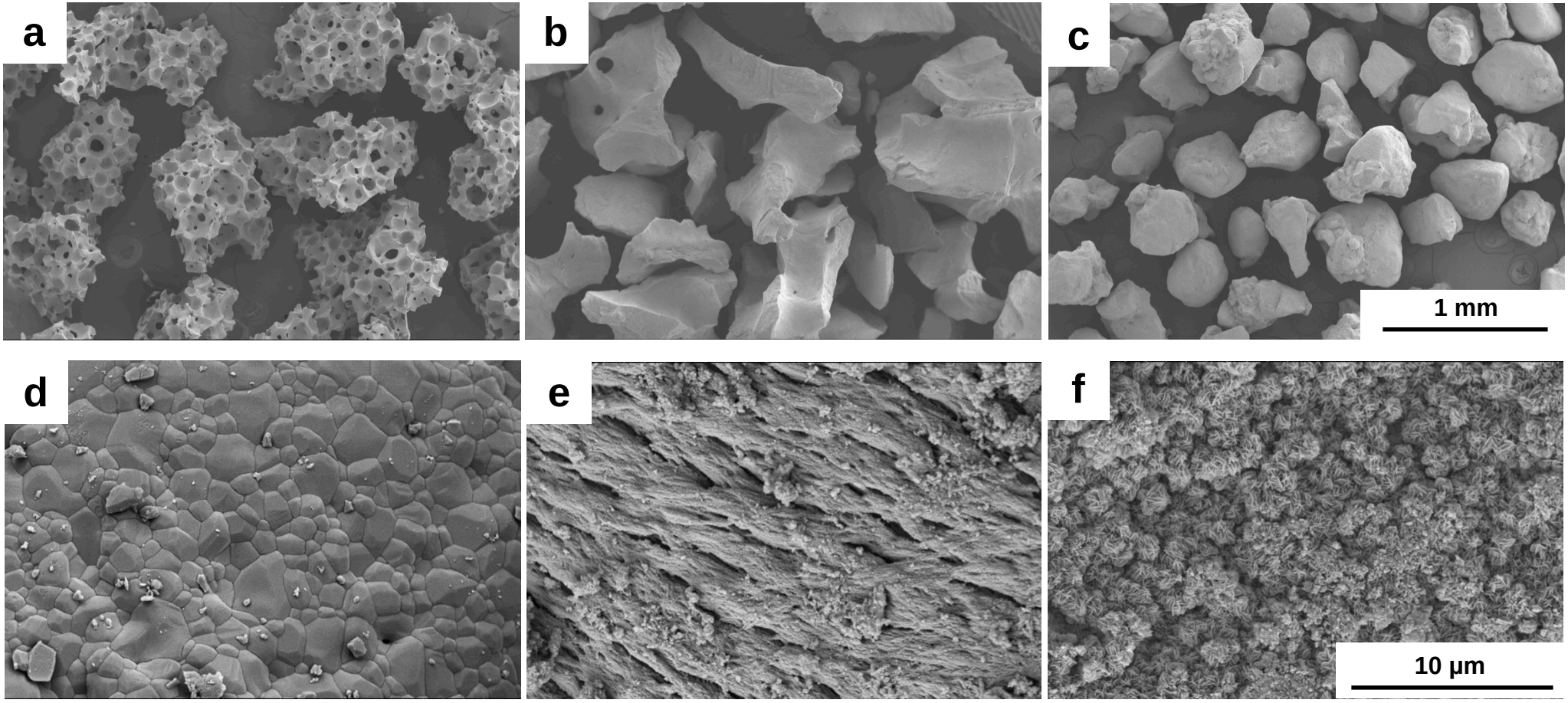
a
b
c
1 mm
d
e
f
10 µm

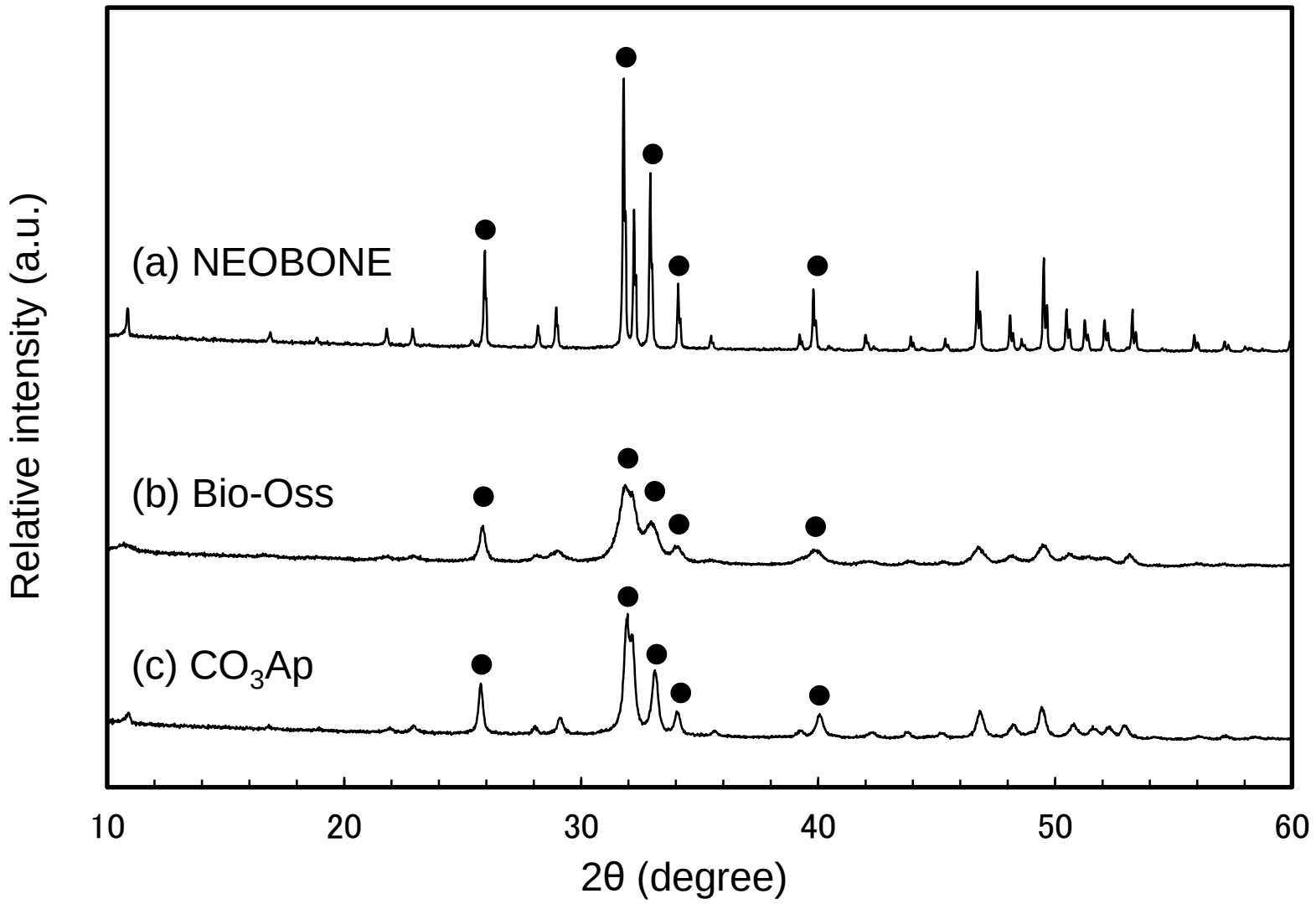
Relative intensity (a.u.)
(a) NEOBONE
(b) Bio-Oss
(c) CO3Ap
10
20
30
40
50
60
2θ (degree)

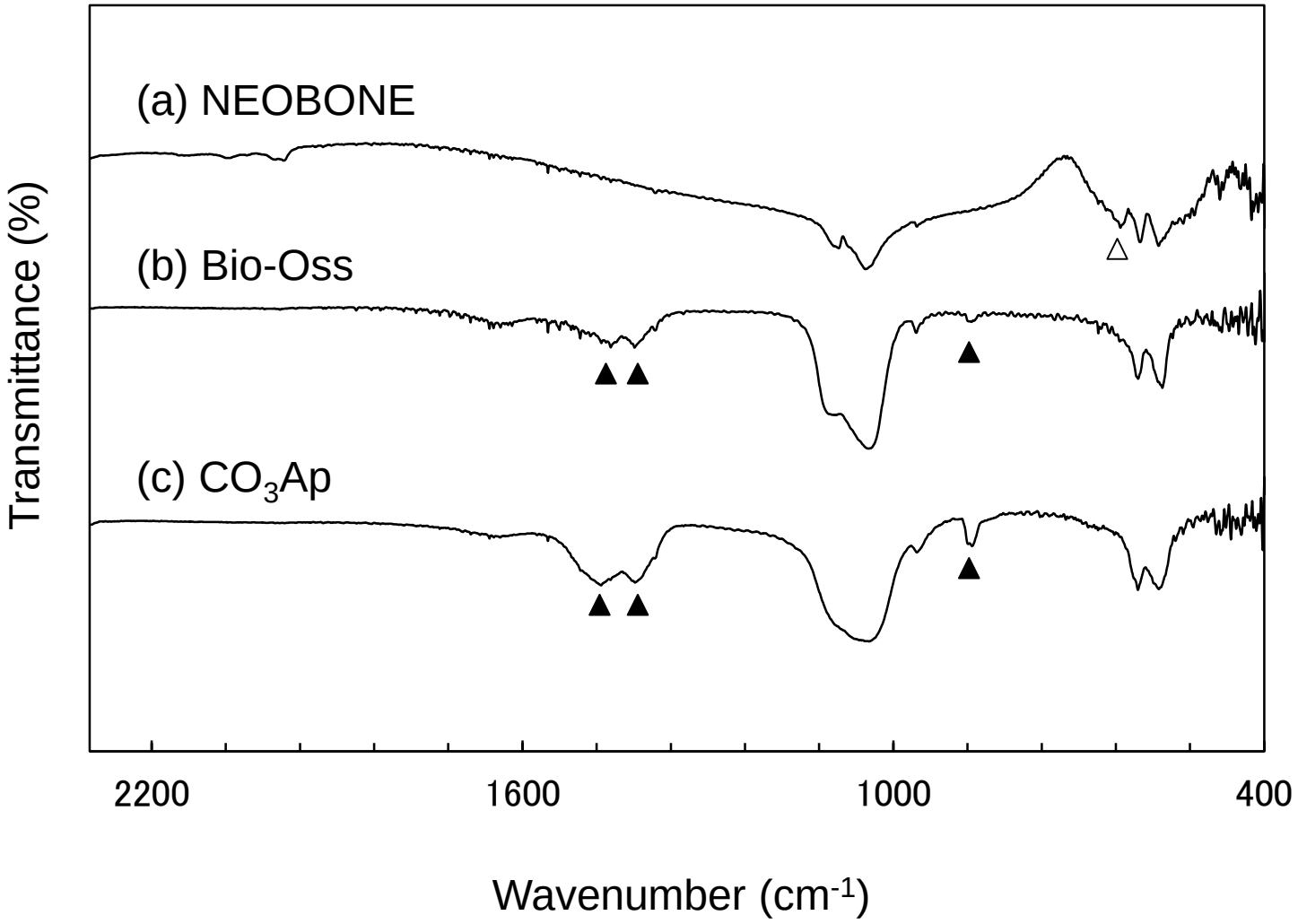
(a) NEOBONE
(b) Bio-Oss
(c) $CO_3Ap$
Transmittance (%)
2200
1600
1000
400
Wavenumber ($cm^{-1}$)

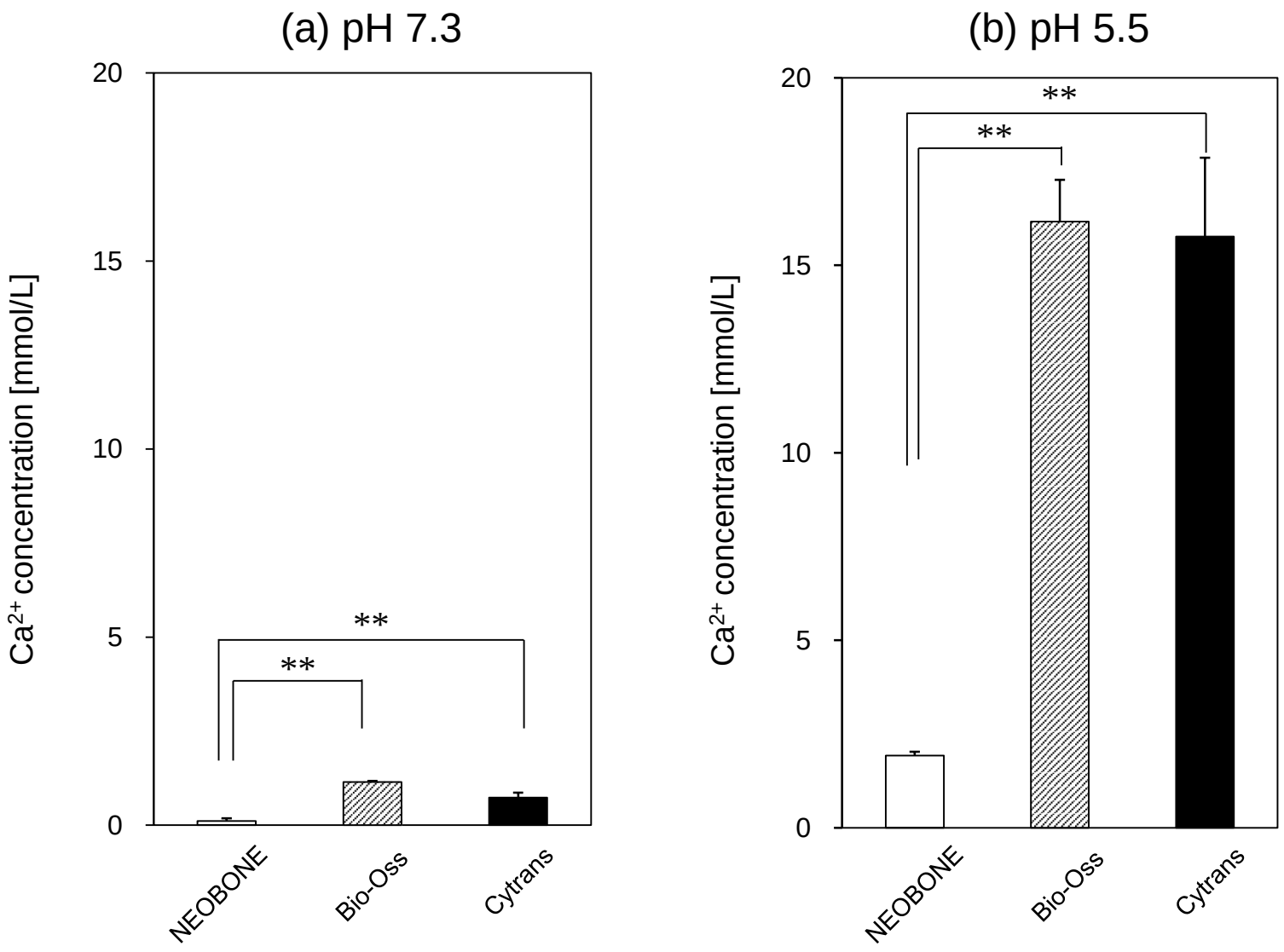
(a) pH 7.3
(b) pH 5.5
Ca2+ concentration [mmol/L]
20
15
10
5
0
**
**
NEOBONE
Bio-Oss
Cytrans

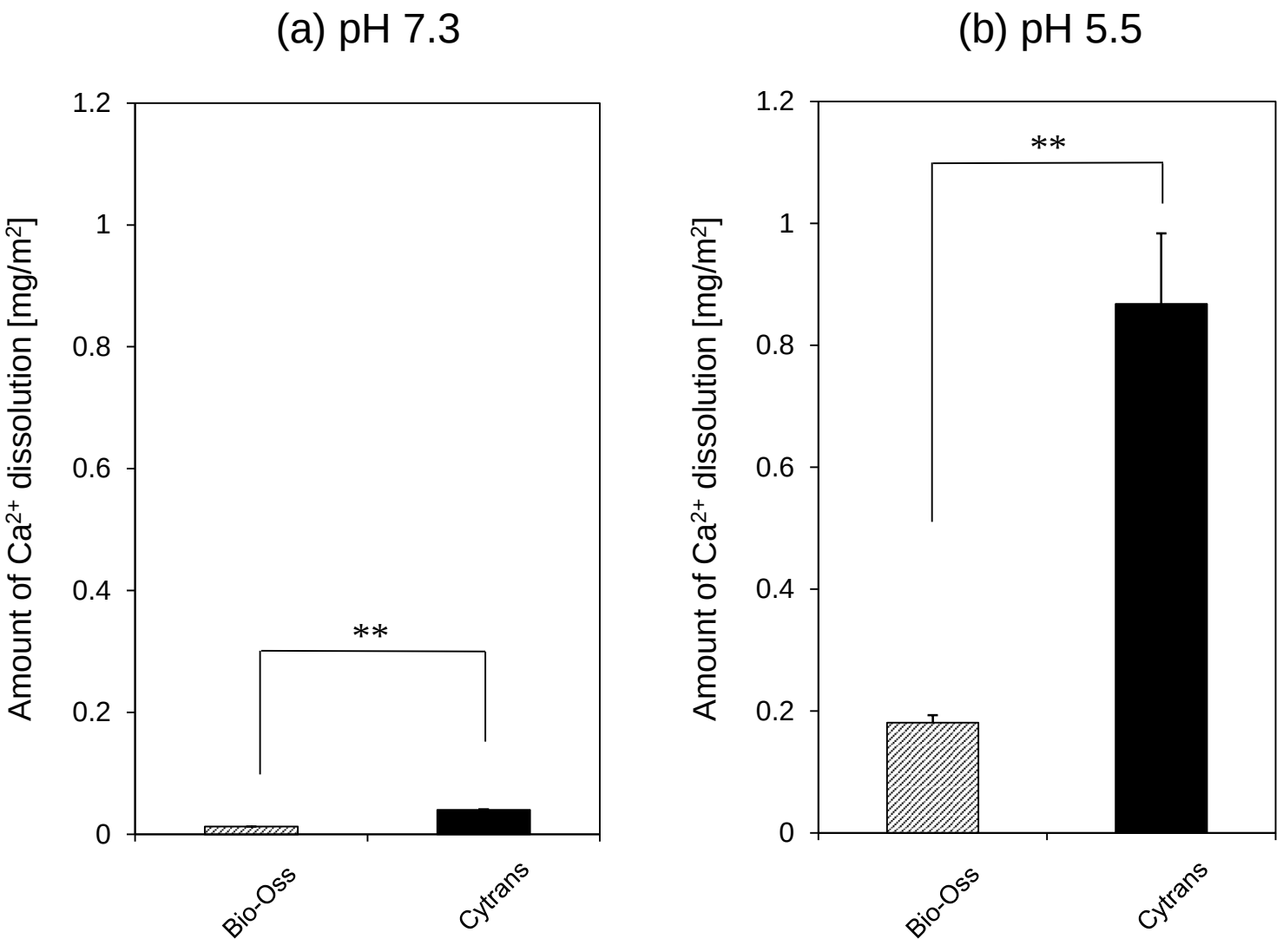
(a) pH 7.3
(b) pH 5.5
Amount of Ca2+ dissolution [mg/m2]
1.2
1
0.8
0.6
0.4
0.2
0
**
Bio-Oss
Cytrans

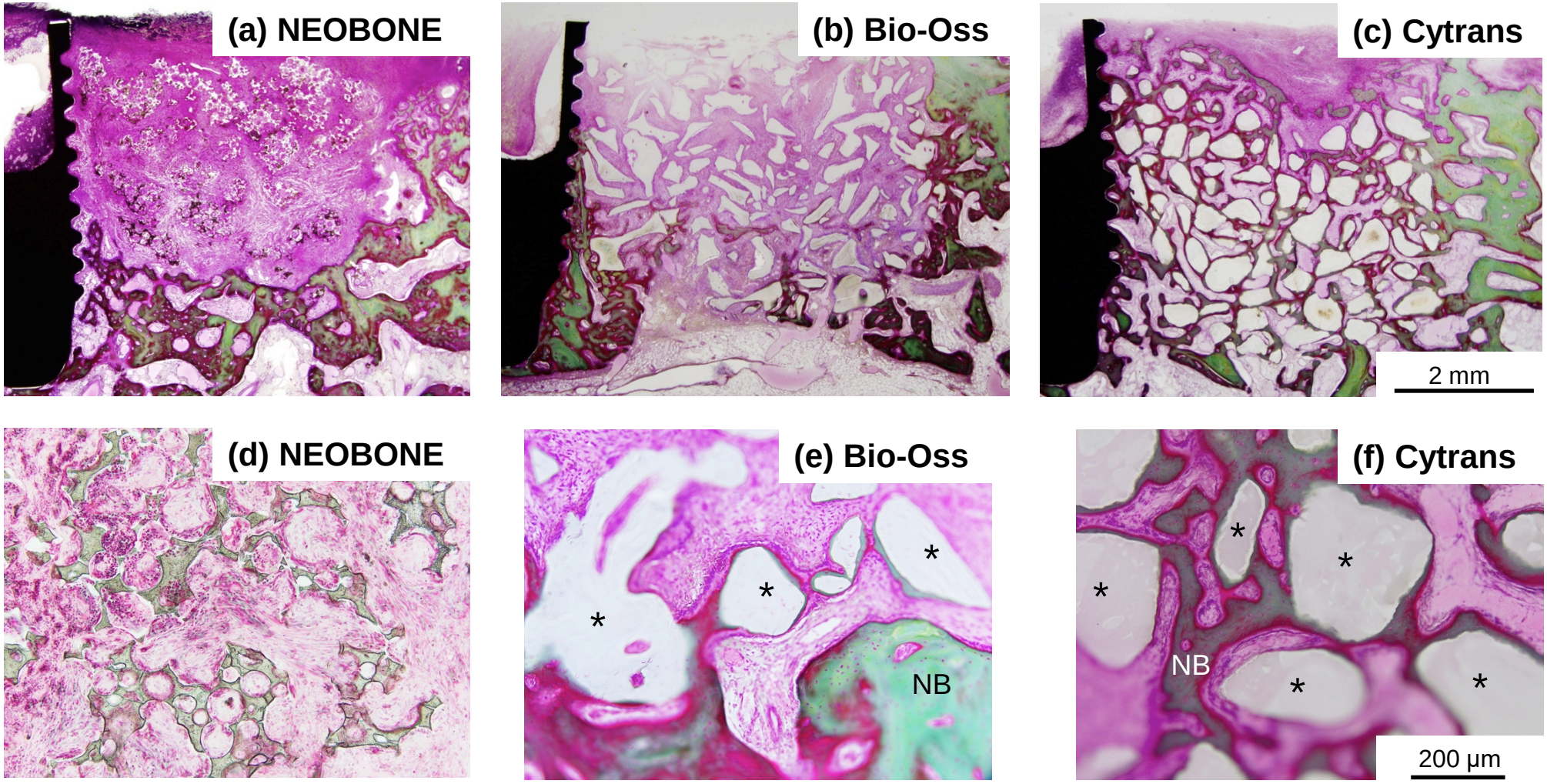
(a) NEOBONE
(b) Bio-Oss
(c) Cytrans
2 mm
(d) NEOBONE
(e) Bio-Oss
NB
(f) Cytrans
NB
200 μm

Table 1 Chemical and physical properties of NEOBONE®, Bio-Oss® and Cytrans®

| Trade name | Type | $CO_3$ content (%) | Crystallite size (nm) | Porosity (%) |
|---|---|---|---|---|
| NEOBONE® | Synthetic | 0.1 ± 0.1 | 76.3 ± 1.3 | not determined |
| Bio-Oss® | Xenograft | 5.5 ± 0.2 | 18.3 ± 1.3 | 57.0 ± 0.5 |
| Cytrans® | Synthetic | 12.0 ± 0.6 | 32.8 ± 1.6 | 25.9 ± 0.7 |

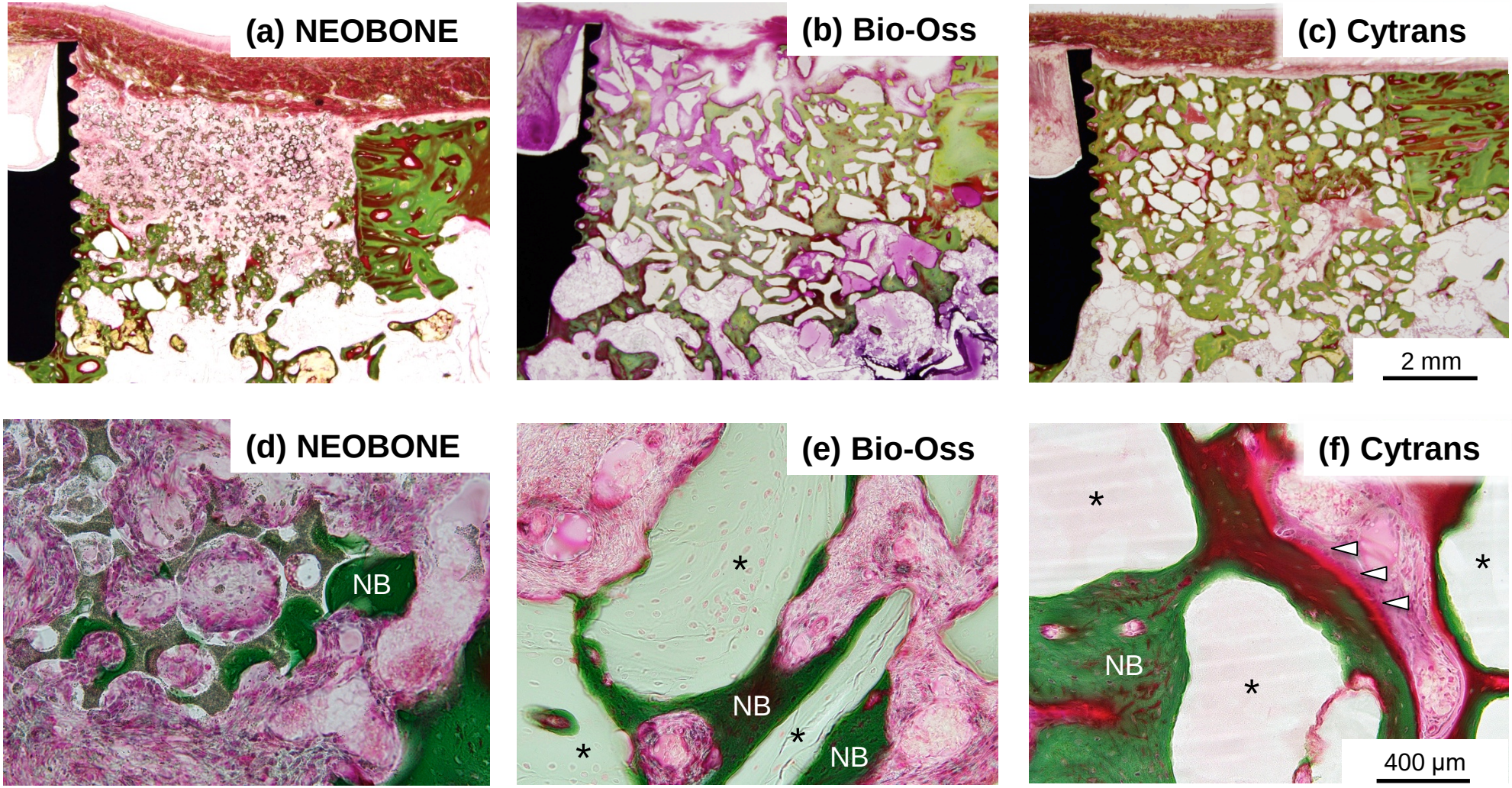
(a) NEOBONE
(b) Bio-Oss
(c) Cytrans
2 mm
(d) NEOBONE
NB
(e) Bio-Oss
NB
NB
*
*
*
(f) Cytrans
NB
*
*
*
400 µm

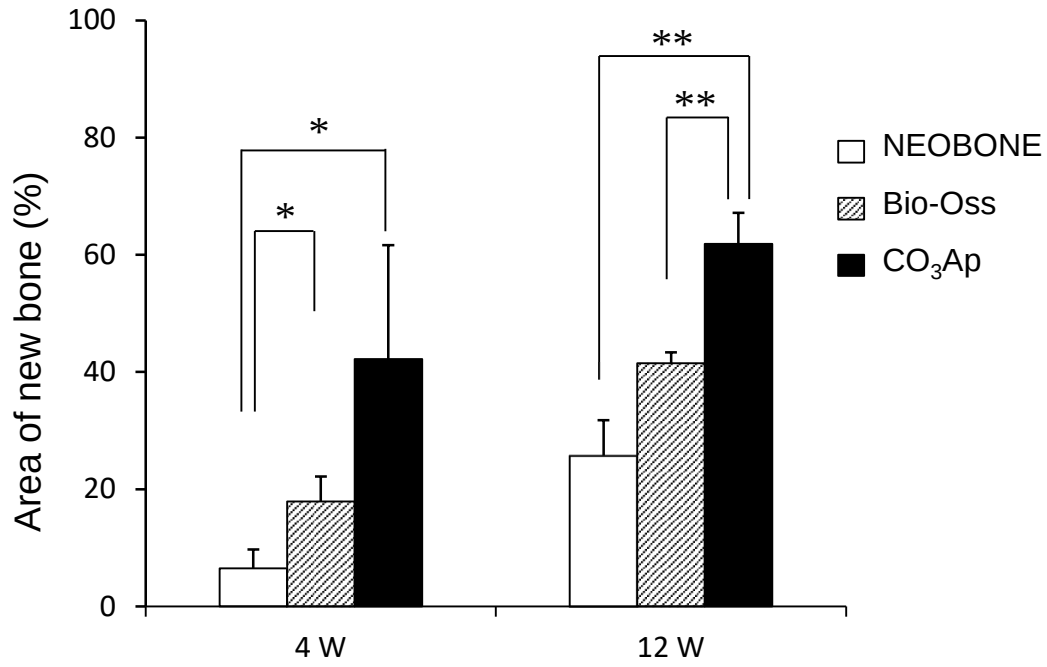
100
80
60
40
20
0
Area of new bone (%)
*
*
**
**
4 W
12 W
NEOBONE
Bio-Oss
CO3Ap

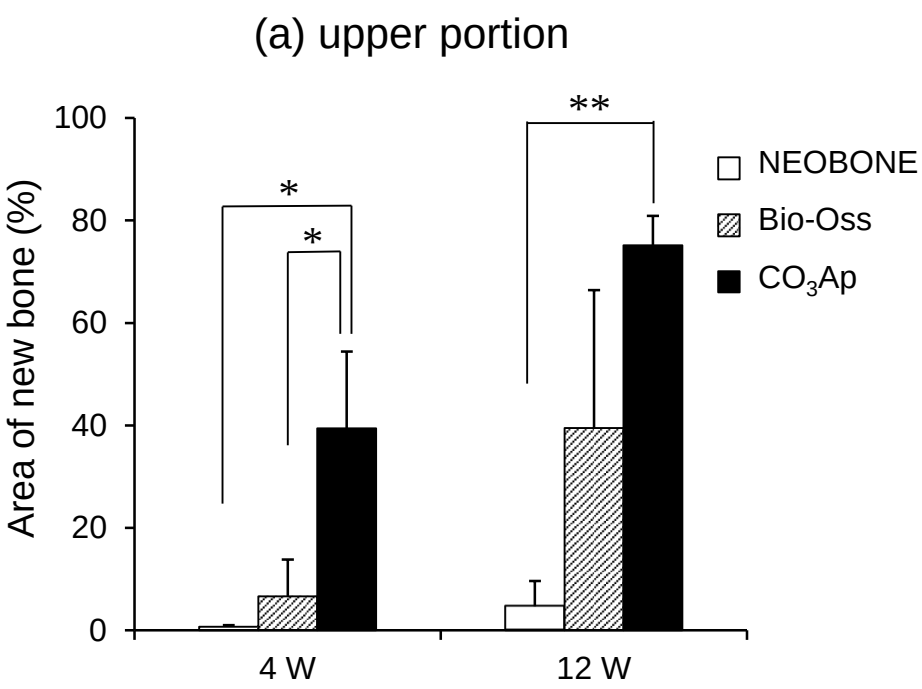
(a) upper portion
Area of new bone (%)
100
80
60
40
20
0
*
*
**
4 W
12 W
NEOBONE
Bio-Oss
CO3Ap

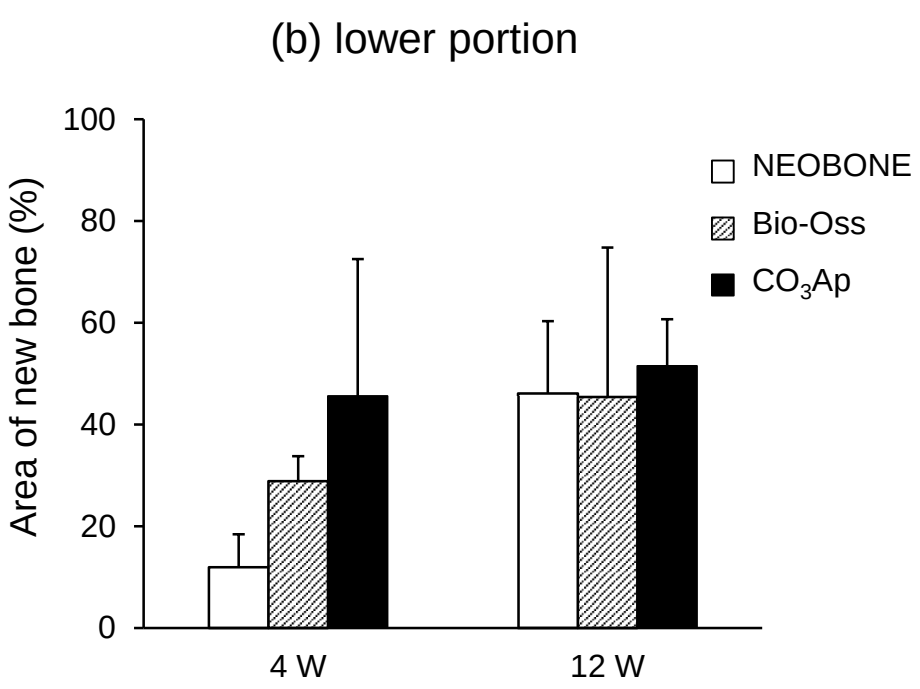
(b) lower portion
Area of new bone (%)
100
80
60
40
20
0
4 W
12 W
NEOBONE
Bio-Oss
CO3Ap

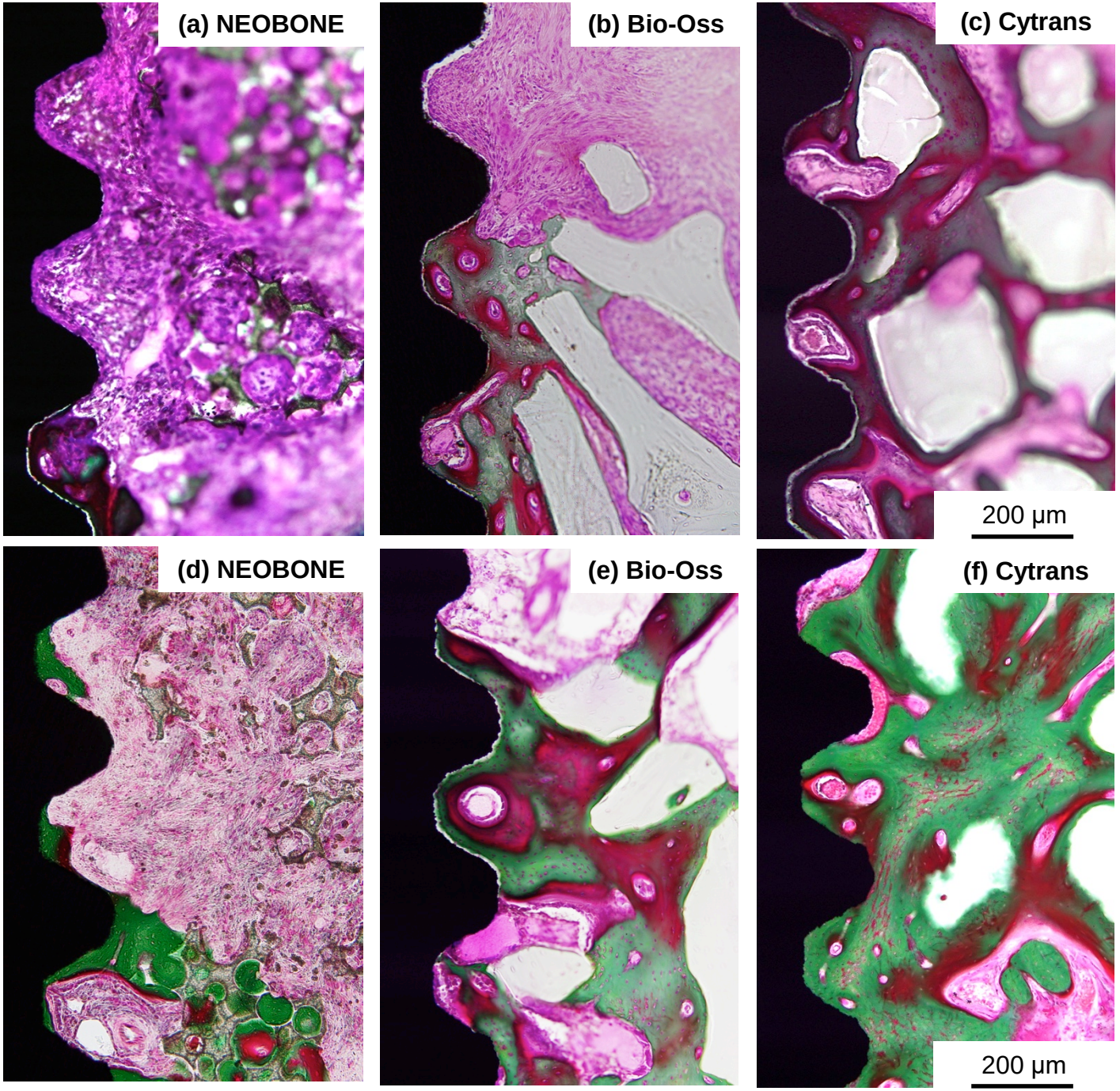
(a) NEOBONE
(b) Bio-Oss
(c) Cytrans
200 µm
(d) NEOBONE
(e) Bio-Oss
(f) Cytrans
200 µm

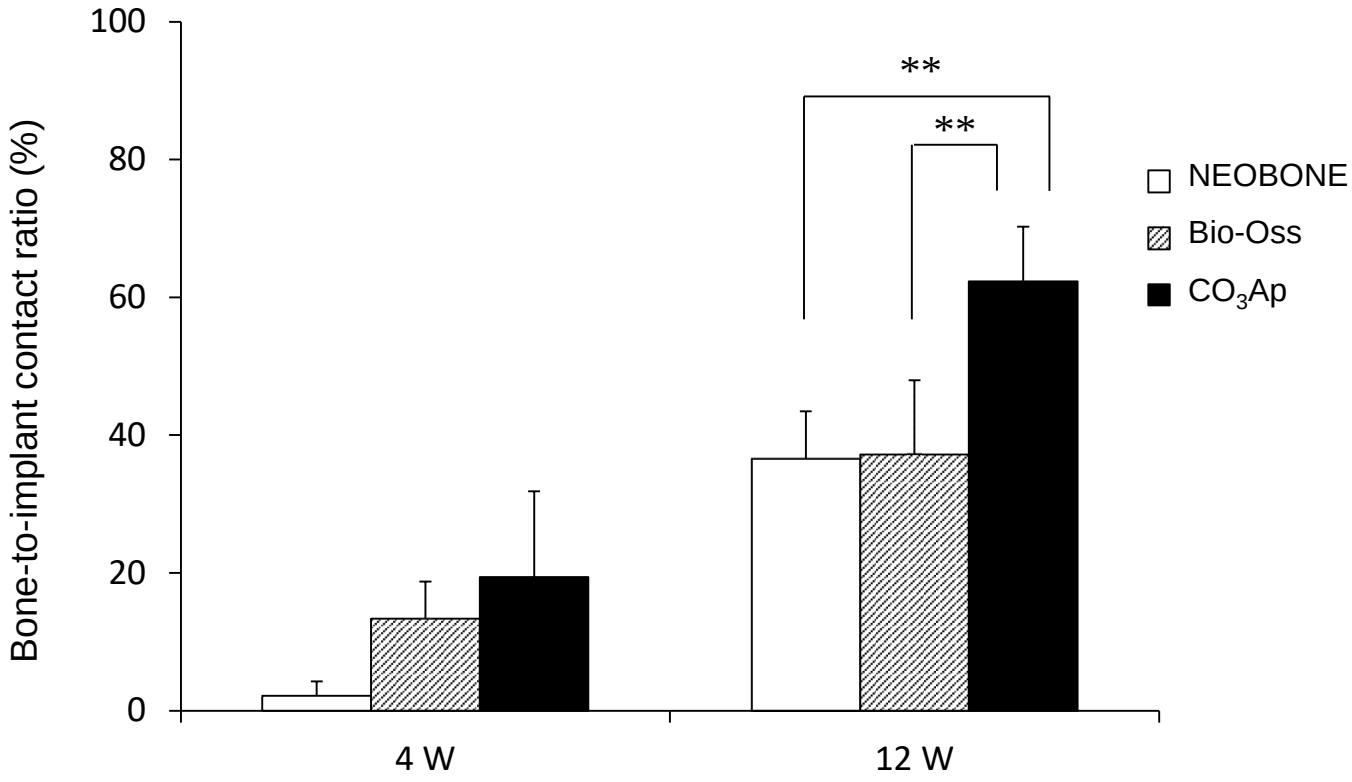
Bone-to-implant contact ratio (%)
100
80
60
40
20
0
**
**
NEOBONE
Bio-Oss
CO3Ap
4 W
12 W

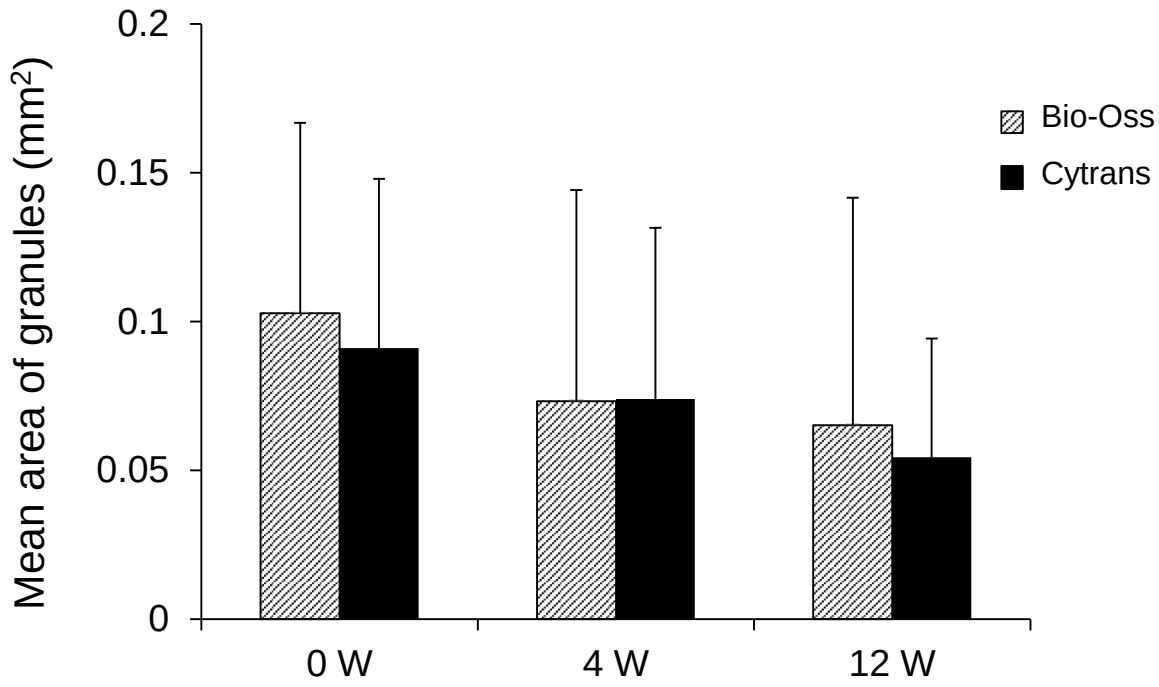
Mean area of granules (mm2)
0.2
0.15
0.1
0.05
0
0 W
4 W
12 W
Bio-Oss
Cytrans